Graphical Abstract

Magnetism and Hyperfine Interactions in the Hexagonal Polymorph of Delafossite $CuFeO_2$

Benedikt Klobes, Manuel Angst, Daniela Fenske, Chinmay Konnur, Abdelfattah Mahmoud, Moulay Tahar Sougrati

Highlights

Magnetism and Hyperfine Interactions in the Hexagonal Polymorph of Delafossite $CuFeO_2$

Benedikt Klobes, Manuel Angst, Daniela Fenske, Chinmay Konnur, Abdelfattah Mahmoud, Moulay Tahar Sougrati

- The hexagonal polymorph of delafossite $CuFeO_2$ was synthesized using a hydrothermal route.
- The magnetic susceptibility generally resembles its counterpart in the rhombohedral polymorph, but transition temperatures are increased.
- Mössbauer measurements reveal magnetic relaxations above the first transition temperature in contrast to the rhombohedral polymorph.
- In the hexagonal phase of $CuFeO_2$, three different magnetic regimes can be dinstinguished at low temperatures.

Magnetism and Hyperfine Interactions in the Hexagonal Polymorph of Delafossite $CuFeO_2$

Benedikt Klobes[a,*], Manuel Angst[b], Daniela Fenske[c], Chinmay Konnur[a], Abdelfattah Mahmoud[d], Moulay Tahar Sougrati[e]

[a] *Bremerhaven Institute of Nanotechnology, University of Applied Sciences Bremerhaven, An der Karlstadt 8, Bremerhaven, 27568, Germany*
[b] *Jülich Centre for Neutron Science JCNS and Peter Grünberg Institute PGI, JARA-FIT, Forschungszentrum Jülich GmbH, Jülich, 52425, Germany*
[c] *Fraunhofer Institute for Manufacturing Technology and Advanced Materials, Wiener Str. 12, Bremen, 28359, Germany*
[d] *GREEnMat, UR CESAM, University of Liège, Allée du Six Août 13, Liège, 4000, Belgium*
[e] *Institut Charles Gerhardt Montpellier, UMR 5253 CNRS-UM-ENSCM, 1919, route de Mende, Montpellier, 34293 cedex 5, France*

Abstract

The magnetic susceptibility of and hyperfine interactions in the hexagonal 2H polymorph of delafossite $CuFeO_2$ were investigated by SQUID magnetometry and Mössbauer spectroscopy, respectively, at low temperatures. The hydrothermally synthesized 2H-$CuFeO_2$ sample contained a 10 vol-% α-Fe_2O_3 impurity detected by X-ray diffraction, whose contribution to the susceptibility and hyperfine interactions were easily distinguishable from the major 2H-$CuFeO_2$ one. Morphology and indirect optical band gap investigated by scanning electron microscopy and diffuse reflectance measurements showed well expected results for a hydrothermally synthesized delafossite sample. The magnetic susceptibility of 2H-$CuFeO_2$ revealed a first antiferromagnetic like transitions at 16 K and a second transition at 13.5 K or 10 K depending on measurement protocol, which points towards modified exchange interactions as compared to the R3 polymorph. Complementary Mössbauer measurements revealed complicated spectral shapes at low temperatures indicating rather complex magnetic structures and magnetic relaxations above

* *Email address:* bklobes@hs-bremerhaven.de (Benedikt Klobes)

20 K.

Keywords: delafossite, $CuFeO_2$, Mössbauer spectroscopy, magnetic susceptibility 76.80.+y, 75.30.Cr, 61.05.C-, 75.50.Ee

---

1. Introduction

Delafossite compounds are oxides of the type $A^{I}B^{III}O_2$, where A is a monovalent cation such as Cu, Ag, and Pd, and B represents trivalent metal ions such as Al, Co, and Fe, with the archetype and original eponym $CuFeO_2$. Two polymorphs of delafossite compounds exist, a rhombohedral (R3) and hexagonal (2H) form with $R\overline{3}m$ and $P6_3/mmc$ space group, respectively [1], which differ in the stacking orientation of the double layers consisting of edge sharing $B^{III}O_6$ octahedra and of triangularly arranged A^{I} layers.

In general, delafossite materials exhibit an interesting and favorable combination of properties which drives research into diverse application areas ranging from thermoelectrics [2] and Li-ion batteries [3] to pollutant degradation [4] and solar energy conversion [5]. Besides, delafossites in general and $CuFeO_2$ in particular exhibit very interesting magnetic properties with complex ordering phenomena and geometric frustration at low temperatures [6, 7, 8, 9, 10]. As the synthesis of the 2H polymorph is challenging and most approaches, including solid state reactions, sol-gel techniques and hydrothermal methods, yield pure or predominantly R3 phase materials [11, 12, 13], the magnetic properties of the 2H polymorphs are much less investigated. This is particularly true for $CuFeO_2$, for which, to the best of the authors' knowledge, the synthesis of the 2H polymorph without R3 contribution has rarely been reported [14, 15] and, thus, the 2H magnetic properties are unknown.

Herein, we report on an investigation of the hexogonal polymorph of delafossite $CuFeO_2$ using a sample obtained by hydrothermal synthesis and methodically based on X-ray diffraction, diffuse optical reflectometry, scanning electron microscopy, SQUID magnetometry and Mössbauer spectroscopy. Low temperature measurements of the magnetic susceptibility and the Mössbauer effect allowed for shining some light on the magnetism in 2H-$CuFeO_2$ which contrasts with the well established one in R3-$CuFeO_2$.

2. Experimental Methods and Synthesis

For synthesis of 2H-$CuFeO_2$, a hydrothermal method, which was previously used for the production of mostly 3R phase delafossite[16, 17, 13], was

modified. In detail, 2.1 mmol of $CuSO_4 \cdot 5H_2O$ (obtained from Alfa Aesar, purity 99 %) was dissolved in 10 ml deionized water, stirred for 10 min, followed by the addition of 2.1 mmol of $FeSO_4 \cdot 7H_2O$ (obtained from Alfa Aesar, purity 99 %) and another 10 min of stirring. Subsequently, 159 mmol of NaOH were added and the mixture was stirred for another 20 min. The solution was then transferred into a 100 ml Polytetrafluoroethylene (PTFE) lined autoclave and stored at 180°C for 24 h. The autoclave cooled down to room temperature naturally and the black product was washed two times using deionized water, once using ethanol and centrifuged at about 5000g for 5 min after each washing step. Eventually, the moist product/powder was dried in air at 60°C for 24 hours.

For band gap determination, the ultraviolet-visible (UV-VIS) diffuse reflectance R_∞ of the sample from 400 to 1100 mm was measured using a VIS spectrometer (Avantes, AvaSpec-ULS2048CL) and a Deuterium-Halogen light source (Avantes, AVALIGHT-DHC). PTFE was used as a reflectance reference material. The optical absorption coefficient α was estimated by the quantity $F(R_\infty)$ according to the Schuster-Kubelka-Munk formula $F(R_\infty) = (1 - R_\infty)^2/(2R_\infty)$ [18, 19].

The phases of the 2H-$CuFeO_2$ powder sample were investigated by X-ray diffraction (XRD) over the 2θ range from 10° to 80° with a Bruker D8 Discover Twin-Twin advance diffractometer using Cu K_α (doublet) radiation. Diffractograms were analyzed by Rietveld refinement using the software Jana2006 [20].

Iron-57 Mössbauer spectra were obtained in transmission mode on a constant acceleration spectrometer using a ^{57}Co/Rh source. Measurements were made using a vibration decoupled closed-cycle He cryostat system. The sample was first cooled down to 6 K (in zero magnetic field) and Mössbauer spectra were collected upon warming. All isomer shifts herein are reported with respect to α-Fe. Mössbauer spectra were analyzed using a program with diagonalization of the complete Hamiltonian and Lorentzian lineshapes (see Sec. 4).

For scanning electron microscopy (SEM) imaging, a Phenom proX instrument with a 4-quadrant backscatter electron detector was used.

The magnetic susceptibility was measured by SQUID magnetometry on a Magnetic Properties Measurement System by Quantum Design. The sample was first cooled down to base temperature in zero field, then a field of 100 Oe was applied and data were measured upon warming (zero-field-cooled, zfc) with a rate of 1 K/min to 50 K, followed by data collection upon cooling

to base temperature again (field-cooled-cooling, fcc) and finally warming to room temperature (field-cooled-warming, fcw).

3. Results and Discussion

The XRD pattern of the investigated 2H-$CuFeO_2$ sample is shown in Fig. 1 including the refinement, and the respective quality factors. The sample consists of 2H-$CuFeO_2$ with a 10(1) vol-% α-Fe_2O_3 impurity phase but without any discernible contribution of the R3 polymorph. This amount of α-Fe_2O_3 equals 9.6(9) mass-% and entails that 10(4) % of all Fe atoms are located in the α-Fe_2O_3 impurity (both relevant for comparison with magnetometry and Mössbauer results, see below). For the 2H phase, fitted lattice

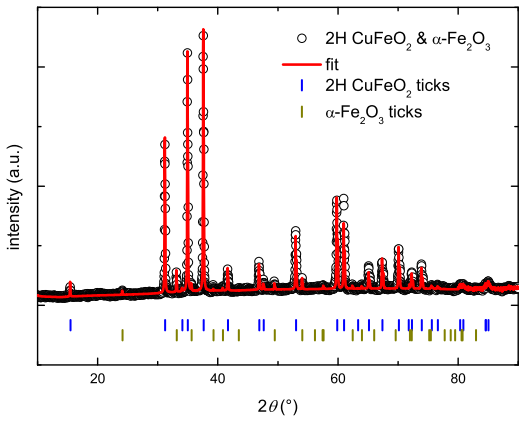

Figure 1: X-ray diffraction pattern of the hydrothermally synthesized $CuFeO_2$ sample. The upper blue tics represent XRD peaks corresponding to 2H-$CuFeO_2$ and the lower green tics correspond to hematite. The weighted profile R-factor of the fit is $R_{wp} = 7.53$ and the goodness of fit equals 1.5.

constants are a = 3.034(2) Å and c = 11.444(3) Å and for α-Fe_2O_3 a = 5.035(3) Å and c = 13.746(3) Å which are in good agreement with literature with respect to both phases [14, 21]. In terms of phase purity, this sample is the best result of the hydrothermal route outlined in Sec. 2. However, the difference between the magnetism in α-Fe_2O_3 and the magnetism in 2H-$CuFeO_2$ turned out to be big enough, not to affect the investigation presented herein. Nonetheless, it should be noted that the hydrothermal synthesis of pure 2H-$CuFeO_2$ was reported in Ref. [15] which could not be reproduced presumably due to problems in replicating water purification and degassing.

A SEM image of the synthesized powder is shown in Fig. 2. The powder consists of platelets with diameter ranging from 500 to 1000 nm, which is a common result for hydrothermally syntesized $CuFeO_2$ samples [22, 15, 23, 13].

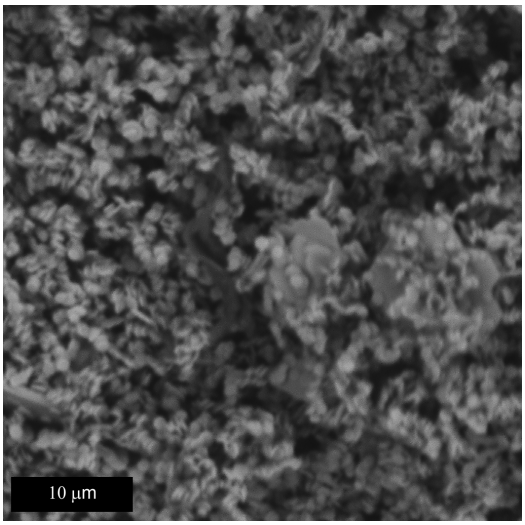

Figure 2: Scanning electron microscopy image of the 2H-$CuFeO_2$ sample. The vast majority of platelets ranges between 500 and 1000 nm.

Additionally, the light absorption of the sample was investigated for band gap determination based on the Tauc-Plot approach (see Sec. 2). Fig. 3 shows the corresponding Tauc plot for an indirect band gap. The band gap value was determined to be 1.37(2) eV, which is reasonably close to the value reported in Ref. [15] and also similar to the range of indirect band gap values reported for the R3 phase [24, 25, 26, 27, 13].

The susceptibility of the sample measured in 100 Oe is shown in Fig. 4. The step visible around 260 K can be attributed to the Morin transition of the α-Fe_2O_3 impurity already deduced from XRD. The temperature of the Morin transition at about 263 K is in good agreement with published values [28]. Comparing the height of the (Morin) step with literature [29], the α-Fe_2O_3 impurity is estimated to contribute about 7 mass-%, which is only slightly lower than the XRD based estimate. The paramagnetic state below the Morin transition was fitted using a Curie-Weiss law (see inset to Fig. 4 top part) yielding a Curie-Weiss temperature $\theta_{CW} = -105(2)$ K and an effective magnetic moment (in the paramagnetic regime) $\mu_{eff} = 5.65(1)\mu_B$

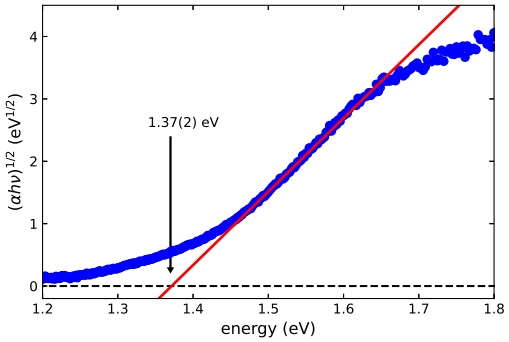

Figure 3: Tauc plot based on the diffuse reflectance of the 2H-$CuFeO_2$ sample. The band gap value is identified as intersection of the linear fit with the baseline.

with the Bohr magneton μ_B. The Curie-Weiss temperature is very close to the one of -110 K reported for R3-$CuFeO_2$ [16] and the determined μ_{eff} is within the usual range expected for high-spin Fe^{+3} [30]. Except for the contribution of the Morin transition due to the α-Fe_2O_3, the susceptibility generally resembles results obtained for the R3 phase of $CuFeO_2$ [31, 16, 23] and other magnetic delafossites [10]. At low temperatures, the paramagnetic increase of χ is replaced by a broad cusp around 20 K and a shoulder at about (and below) 15 K on the falling slope of the magnetic susceptibility. In R3-$CuFeO_2$ these features correspond to a first transition at $T_{1,R3}$ from the paramagnetic state to a quasi-longe-range ordered, sinusoidally amplitude modulated, incommensurate magnetic structure and a subsequent transition to a commensurate antiferromagnetic structure below $T_{2,R3}$ [32, 6]. Transition temperature values for R3-$CuFeO_2$ are rather consistently reported to be $T_{1,R3} \approx 13$ K and $T_{2,R3} \approx 10$ K (see Tab. 1). In 2H-$CuFeO_2$ however, magnetic transition temperatures $T_{(1,2),2H}$ are significantly shifted towards higher temperatures (see Tab. 1) as determined by the maximum of the temperature derivative of the susceptibility, $\frac{d\chi}{dT}$ (see inset to the lower part of Fig. 4). Note that zero-field cooled and field cooled warming curves are almost identical except for a small difference below 10 K, which could be caused by the α-Fe_2O_3 impurity [33]. A similar shift of transition temperatures was reported for the R3 and 2H phases of the related delafossite $AgFeO_2$ [10, 34] and attributed to modified exchange interactions due to different stacking sequences of Fe^{+3} layers [34]. Notably however, this analogy should not be overstretched as the low temperature magnetic structures of R3-$CuFeO_2$ and R3-$AgFeO_2$ significantly differ with the latter exhibting a

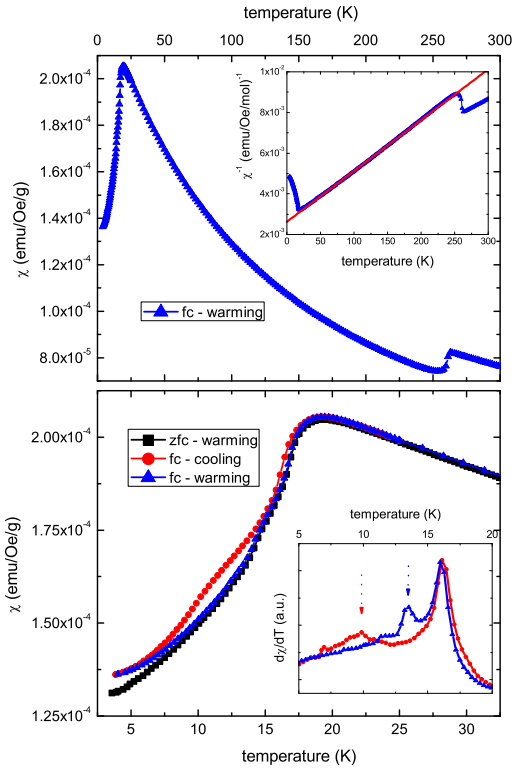

Figure 4: (top) Temperature dependent susceptibility measured during warming after field cooling from 4 K to room temperature. Note the Morin transition due to the impurity phase.The inset shows the inverse susceptibility and a Curie-Weiss fit for Neel-temperature determination (see text for further details). (bottom) Low temperature part of the susceptibility revealing differences between field cooled warming and zero field cooled warming. The inset shows the temperature derivative of the susceptibilty, which is used for quantification of the magnetic transition temperatures (see arrows for the lower transition).

cycloid magnetic order [34] below the respective $T_{2,R3}$ (and not an Ising-like antiferromagnetic order as R3-$CuFeO_2$). Moreover in 2H-$CuFeO_2$, there is clear thermal hysteresis for the lower transition, i.e., $T_{2,2H,fcc} = 9.9$ K upon field cooled cooling measurements and $T_{2,2H,fcw} = 13.5$ K obtained by susceptibility measurements during warming after field cooling.

In order to obtain microscopic insight into the magnetism of 2H-$CuFeO_2$ low temperature Mössbauer spectroscopy measurements using the ^{57}Fe nuclear resonance were carried out and the results are shown in Fig. 5. Mössbauer spectra measured at 240 and 270 K exhibit two well discriminable features, *i.e.*, a doublet with isomer shift of 0.37(1) mm/s and quadrupole

info	$T_{1,info}$ (K)	$T_{2,info}$ (K)	method	source
2H fcc	16.1	9.9	magnetometry	this work
2H fcw	16.0	13.5	magnetometry	this work
2H MB	20	16	Mössbauer	this work
R3	12.5	10.0	magnetometry	[23]
R3	14.0	10.5	neutron diffraction	[32]
R3	13.0	9.0	magnetometry	[31]
R3	n.a.	10.0	Mössbauer	[35]

Table 1: Magnetic transition temperatures of the 2H and R3 polytypes of $CuFeO_2$ obtained by different methods. The abbreviations fcc and fcw indicate field cooled cooling and field cooled warming curves, respectively (see also Sec. 2 for details). Mössbauer (MB) measurements presented herein were performed upon warming after zero field cooling.

splitting of 0.62(1) mm/s and a magnetically split sextet with a strong hyperfine field of 54.4(1) T. The doublet and its Mössbauer parameters represent high spin Fe^{3+} in an octahedral setting, which is expected considering the 2H crystal structure, and the sextet corresponds to the α-Fe_2O_3 impurity phase [36] with a relative contribution of about 14% to the Mössbauer spectra (see also Tab. 2). Due to the presumably high Lamb-Mössbauer factor of α-Fe_2O_3, this contribution is slightly higher than the one determined by XRD at high temperatures but decreases to about 10% at low temperatures in agreement with the XRD estimate. At and below 26 K, the Mössbauer spectra become significantly more complex, *i.e.*, at the expense of the doublet rather complex magnetically split spectra develop whose shape slightly simplify with decreasing temperature. In the case of R3-$CuFeO_2$, similarly complex spectra were measured using classical Mössbauer spectroscopy [35, 23] and nuclear forward scattering (NFS) [9] particularly due to the intermediate magnetic phase between the two transition temperatures. However, the magnetic transition temperatures of the rhombohedral phase inferred from Mössbauer spectroscopy and NFS closely matches their macroscopic counterparts [35, 9, 23], which is obviously not that case for 2H-$CuFeO_2$ exhibiting magnetically affected components well above 20 K. This is also illustrated by the average hyperfine magnetic field (see Fig. 6, further details concerning its determination are discussed below), which at 20 K just starts decreasing until about 26 K. For analyzing the Mössbauer spectra, a conservative fitting approach of using as few discrete magnetically split components as possible was selected. Additionally, the parameters of the sextet corresponding to α-

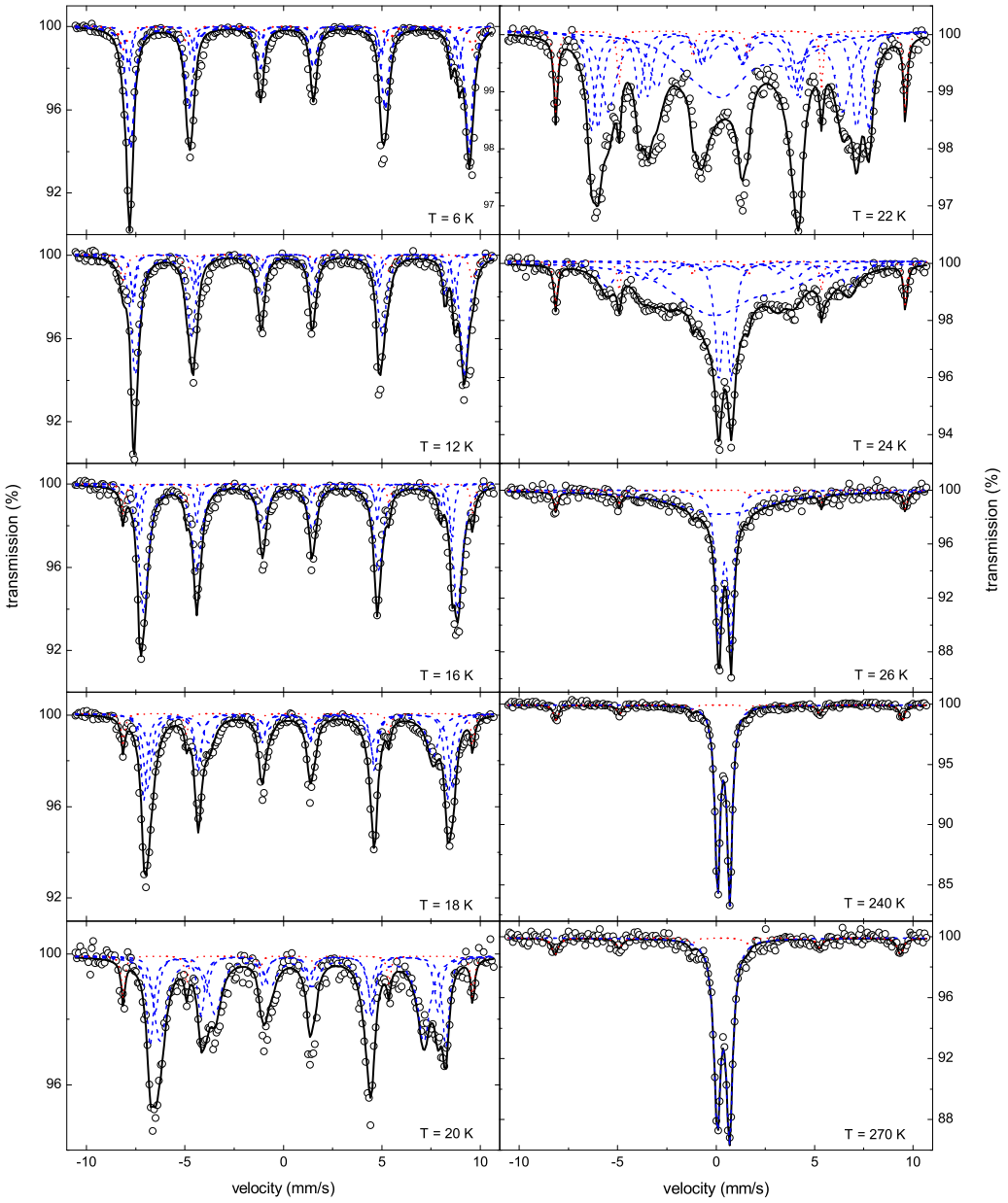

Figure 5: Mössbauer spectra of 2H-$CuFeO_2$ with a minor α-Fe_2O_3 impurity. Black lines represent the fit, red dotted lines represent the α-Fe_2O_3, and blue dashed lines represent the different components used to fit the contribution of 2H-$CuFeO_2$. See also Tab. 2 for details.

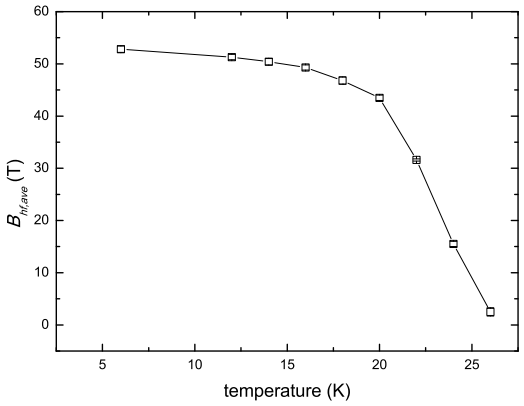

Figure 6: Average hyperfine field $B_{hf,ave}$ in 2H-$CuFeO_2$ calculated using the relative contributions and hyperfine fields of the different components as summarized in Tab. 2.

Fe_2O_3 were fixed for fitting spectra obtained below 26 K, in order to reduce the number of fit parameters. The results of all fits are summarized in Tab. 2 and shown in Fig. 5. In contrast to both the susceptibility measurements presented herein and to published Mössbauer results concerning R3-$CuFeO_2$ [35, 23], the assignment of magnetic transition temperatures using the measured Mössbauer spectra is not trivial. Broad and unresolved components exhibiting significant linewidths of 1 mm/s or more in combination with hyperfine magnetic fields below 10 T are required to model spectra measured from 26 to 22 K. Such fitted parameters most likely do not reflect the actual microscopic situation, but rather represent a relaxation of the hyperfine field and short range correlations affecting the Mössbauer transition within this temperature range. A similar observation of unresolved components above the respective first transition temperature was reported for delafossite R3-$AgFeO_2$ [37]. Spectra measured at 20 and 18 K can be fitted using rather clearly resolved, magnetically split components, which contribute evenly to the overall spectral shape. On the contrary, the fits of Mössbauer data obtained at 16 K and below are dominated by one of the three used components. Thus, the width of the hypothetical hyperfine field distribution decreases with decreasing temperature. From a microscopic perspective, the transition temperatures thus seem to be even higher at about 20 and 16 K, respectively (see Tab. 1). As the narrowing of the hyperfine field distribution (or, paraphrased, the increase of the contribution of a single component) was also observed in R3-$CuFeO_2$ [35, 23] and R3-$AgFeO_2$ [37], this may indicate a

likewise transition from a complex spin density wave like magnetic structure to a less complex, potentially antiferromagnetic one with decreasing temperature. Moreover, some additional complexity with respect to hyperfine parameters can be attributed to the sample itself. Hydrothermal synthesis is known for facilitating the formation of off-stoichiometries in delafossite as reported for $CuAlO_2$ [38], which in the present case would affect the local environment of the Fe cations and, thus, the Mössbauer parameters. This is further supported by a comparison of Mössbauer spectroscopy results on R3-$CuFeO_2$ samples synthesized using a solid state method at high temperatures [35] or using a hydrothermal approach [23]. In the former case, a single component was sufficient for fitting a Mössbauer spectrum below $T_{1,R3}$, whereas, for the latter sample, two distinct, almost equally contributing components had to be used. Whether such defects are connected to or even facilitate the observed relaxation phenomena, cannot be answered here but requires further investigations.

4. Conclusions

The hexagonal polymorph of $CuFeO_2$ was prepared using a hydrothermal synthesis. X-ray diffraction measurement confirmed that the rhombohedral phase was not formed but a small hematite impurity instead which however did not affect subsequent investigations. Scanning electron microscopy and diffuse reflectance measurement confirmed the rather expectable properties of 2H-$CuFeO_2$ in terms of particle size due to hydrothermal synthesis and indirect optical band gap. The magnetic properties were investigated by SQUID magnetometry and Mössbauer spectroscopy. Although the overall temperature dependence of the magnetic susceptibility resembles the one of the R3 polymorph with an antiferromagnetic like behavior at low temperatures, magnetic transitions occur at higher temperatures, show a thermal hysteresis and differ from microscopic and macroscopic perspectives. Mössbauer spectra showed that magnetic relaxation occurs in 2H-$CuFeO_2$ even above the first (macroscopic) transition temperature, which suggests that there are (at least) three distinct magnetic regimes (beside the ordinary paramagnetic one) at low temperatures in the hexagonal polymorph. In the future, extensive magnetization and neutron diffraction measurements at low temperatures are necessary in order to reveal the microscopic structure of these magnetic phases. Moreover, low temperature X-ray diffraction investigations of the 2H polymorph would be helpful for determining any concomitant structural

phase transitions, which are connected to the magnetic transitions in the R3 phase of $CuFeO_2$ [39, 6].

Acknowledgments

We thank Dr. Raphael Hermann, Oak Ridge National Laboratory, USA, for provision of the Mössbauer analysis program.

References

[1] M. A. Marquardt, N. A. Ashmore, D. P. Cann, Crystal chemistry and electrical properties of the delafossite structure, Thin Solid Films 496 (1) (2006) 146–156. doi:10.1016/j.tsf.2005.08.316.

[2] M. Tato, R. Shimonishi, M. Hagiwara, S. Fujihara, Reactive Templated Grain Growth and Thermoelectric Power Factor Enhancement of Textured CuFeO2 Ceramics, ACS Appl Energy Mater 3 (2) (2020) 1979–1987. doi:10.1021/acsaem.9b02407.

[3] M. Zhang, G. Zhu, J. Dai, X. Zhu, Q. Liu, Q. Li, Fabrication and electrochemical performance of delafossite CuFeO2 particles as a stable anode material for lithium-ion batteries, Journal of Materials Science: Materials in Electronics 29 (22) (2018) 19454–19460. doi:10.1007/s10854-018-0075-0.

[4] C. Dai, X. Tian, Y. Nie, H.-M. Lin, C. Yang, B. Han, Y. Wang, Surface Facet of CuFeO2 Nanocatalyst: A Key Parameter for H2O2 Activation in Fenton-Like Reaction and Organic Pollutant Degradation, Environ Sci Technol 52 (11) (2018) 6518–6525. doi:10.1021/acs.est.8b01448.

[5] Q.-L. Liu, Z.-Y. Zhao, R.-D. Zhao, J.-H. Yi, Fundamental properties of delafossite CuFeO2 as photocatalyst for solar energy conversion, J Alloy Compd 819 (2020) 153032. doi:10.1016/j.jallcom.2019.153032.

[6] F. Ye, Y. Ren, Q. Huang, J. A. Fernandez-Baca, P. Dai, J. W. Lynn, T. Kimura, Spontaneous spin-lattice coupling in the geometrically frustrated triangular lattice antiferromagnet Cu Fe O 2, Physical Review B 73 (22) (Jun. 2006). doi:10.1103/PhysRevB.73.220404.

[7] N. Terada, S. Mitsuda, T. Fujii, D. Petitgrand, Inelastic neutron scattering study of frustrated Heisenberg triangular magnet CuFeO 2, J Phys Condens Mat 19 (14) (2007) 145241. doi:10.1088/0953-8984/19/14/145241.

[8] K. Hayashi, T. Nozaki, R. Fukatsu, Y. Miyazaki, T. Kajitani, Spin dynamics of triangular lattice antiferromagnet CuFeO 2 : Crossover from spin-liquid to paramagnetic phase, Physical Review B 80 (14) (Oct. 2009). doi:10.1103/PhysRevB.80.144413.

[9] B. Klobes, M. Herlitschke, K. Z. Rushchanskii, H.-C. Wille, T. T. A. Lummen, P. H. M. van Loosdrecht, A. A. Nugroho, R. P. Hermann, Anisotropic lattice dynamics and intermediate-phase magnetism in delafossite CuFeO 2, Phys Rev B 92 (1) (Jul. 2015). doi:10.1103/PhysRevB.92.014304.

[10] N. Terada, D. D. Khalyavin, P. Manuel, Y. Tsujimoto, A. A. Belik, Magnetic ordering and ferroelectricity in multiferroic 2H-$AgFeO_2$: Comparison between hexagonal and rhombohedral polytypes, Physical Review B 91 (9) (2015) 094434, publisher: American Physical Society. doi:10.1103/PhysRevB.91.094434.

[11] E. Mugnier, A. Barnabé, P. Tailhades, Synthesis and characterization of CuFeO2+ delafossite powders, Solid State Ionics 177 (5) (2006) 607–612. doi:https://doi.org/10.1016/j.ssi.2005.11.026.

[12] R. F. Wu, W. Pan, S. Liu, J. Li, Synthesis of CuFeO2 Powder by Sol-Gel Method, Key Eng Mater 368-372 (2008) 663–665. doi:10.4028/www.scientific.net/KEM.368-372.663.

[13] N. Igbinehi, A. Mahmoud, D. Fenske, B. Klobes, Doping-Dependent Phase Fractions in Hydrothermally Synthesized Mn-Doped CuFeO2, physica status solidi (a) 219 (2022) 2100713. doi:10.1002/pssa.202100713.

[14] H. Effenberger, Structure of hexagonal copper(i) ferrite, Acta Crystallogr C 47 (12) (1991) 2644–2646. doi:10.1107/S0108270191006790.

[15] Y. Jin, G. Chumanov, Solution synthesis of pure 2H CuFeO2 at low temperatures, RSC Adv 6 (31) (2016) 26392–26397. doi:10.1039/C6RA01901C.

[16] D. Xiong, Y. Qi, X. Li, X. Liu, H. Tao, W. Chen, X. Zhao, Hydrothermal synthesis of delafossite CuFeO2 crystals at 100 °C, RSC Adv 5 (61) (2015) 49280–49286. doi:10.1039/C5RA08227G.

[17] T. Jiang, Y. Zhao, M. Liu, Y. Chen, Z. Xia, H. Xue, Enhancing the Lifetime of Photoinduced Charge Carriers in CuFeO2 Nanoplates by Hydrothermal Doping of Mg for Photoelectrochemical Water Reduction, Phys Status Solidi A 215 (14) (2018) 1800056. doi:10.1002/pssa.201800056.

[18] A. Schuster, Radiation through a foggy atmosphere, Astrophys J 21 (1905) 1–21. doi:10.1086/141186.

[19] P. Kubelka, F. Munk, Ein beitrag zur optik der farbanstriche, Z Techn Physik 12 (1931) 593–601.

[20] V. Petříček, M. Dušek, L. Palatinus, Crystallographic Computing System JANA2006: General features, Z Kris Cryst Mater 229 (5) (2014) 345–352. doi:10.1515/zkri-2014-1737.

[21] R. L. Blake, R. E. Hessevick, T. Zoltai, L. W. Finger, Refinement of the hematite structure, American Mineralogist 51 (1-2) (1966) 123–129.

[22] D. Xiong, Q. Zhang, S. K. Verma, X.-Q. Bao, H. Li, X. Zhao, Crystal structural, optical properties and mott-schottky plots of p-type Ca doped CuFeO2 nanoplates, Mat. Res. Bull. 83 (2016) 141–147. doi:10.1016/j.materresbull.2016.05.031.

[23] K. Siedliska, T. Pikula, Z. Surowiec, R. Panek, R. Idczak, V. H. Tran, E. Jartych, Crystal structure and hyperfine interactions of delafossite (CuFeO2) synthesized hydrothermally, Acta Crystallographica Section B: Structural Science, Crystal Engineering and Materials 77 (4) (2021) 570–576, publisher: International Union of Crystallography. doi:10.1107/S2052520621005072.

[24] F. A. Benko, F. P. Koffyberg, Opto-electronic properties of p- and n-type delafossite, CuFeO2, J Phys Chem Solids 48 (5) (1987) 431–434. doi:10.1016/0022-3697(87)90103-X.

[25] K. P. Ong, K. Bai, P. Blaha, P. Wu, Electronic Structure and Optical Properties of AFeO $_2$ (A = Ag, Cu) within GGA Calculations, Chem Mater 19 (3) (2007) 634–640. doi:10.1021/cm062481c.

[26] Q. Deng, H. Chen, G. Wang, Y. Shen, F. Liu, S. Wang, Structural, optical and photoelectrochemical properties of p type Ni doped CuFeO2 by hydrothermal method, Ceram Int 46 (1) (2020) 598–603. doi:10.1016/j.ceramint.2019.09.008.

[27] Y.-H. Chang, H. Wang, T.-F. Siao, Y.-H. Lee, S.-Y. Bai, C.-W. Liao, J.-K. Zhuang, T.-W. Chiu, C.-H. Kuo, A new solution route for the synthesis of CuFeO2 and Mg-doped CuFeO2 as catalysts for dye degradation and CO2 conversion, J Alloy Compd 854 (2021) 157235. doi:10.1016/j.jallcom.2020.157235.

[28] L. Néel, Some New Results on Antiferromagnetism and Ferromagnetism, Reviews of Modern Physics 25 (1) (1953) 58–63. doi:10.1103/RevModPhys.25.58.

[29] F. Jiao, A. Harrison, J.-C. Jumas, A. V. Chadwick, W. Kockelmann, P. G. Bruce, Ordered mesoporous fe2o3 with crystalline walls, Journal of the American Chemical Society 128 (16) (2006) 5468–5474. doi:10.1021/ja0584774.

[30] S. Mugiraneza, A. M. Hallas, Tutorial: a beginner's guide to interpreting magnetic susceptibility data with the Curie-Weiss law, Communications Physics 5 (1) (2022) 1–12, number: 1 Publisher: Nature Publishing Group. doi:10.1038/s42005-022-00853-y.

[31] H. Takahashi, Y. Motegi, R. Tsuchigane, M. Hasegawa, Pressure effect on the antiferromagnetic transition temperature in CuFeO2, Journal of Magnetism and Magnetic Materials 272-276 (2004) 216–217. doi:10.1016/j.jmmm.2003.11.084.

[32] S. Mitsuda, N. Kasahara, T. Uno, M. Mase, Partially disordered phase in frustrated triangular lattice antiferromagnet CuFeO 2, Journal of the Physical Society of Japan 67 (12) (1998) 4026–4029.

[33] S.-J. Lee, H. Jung, S. Lee, J. Dho, Superparamagnetic behaviour of reentrant weak-ferromagnetic phase in haematite crystal at low temper-

atures, New Journal of Physics 11 (2) (2009) 023020. doi:10.1088/1367-2630/11/2/023020.

[34] N. Terada, Y. Ikedo, H. Sato, D. D. Khalyavin, P. Manuel, F. Orlandi, Y. Tsujimoto, Y. Matsushita, A. Miyake, A. Matsuo, M. Tokunaga, K. Kindo, Difference in magnetic and ferroelectric properties between rhombohedral and hexagonal polytypes of AgFeO 2 : A single-crystal study, Physical Review B 99 (6) (2019) 064402. doi:10.1103/PhysRevB.99.064402.

[35] D. H. Choi, I.-B. Shim, C. S. Kim, Mössbauer study of antiferromagnetic CuFeO2, Journal of Magnetism and Magnetic Materials 320 (20) (2008) e575–e577. doi:10.1016/j.jmmm.2008.04.018.

[36] F. van der Woude, Mössbauer effect in -fe2o3, physica status solidi (b) 17 (1) (1966) 417–432. doi:https://doi.org/10.1002/pssb.19660170147.

[37] A. Sobolev, V. Rusakov, A. Moskvin, A. Gapochka, A. Belik, I. Glazkova, A. Akulenko, G. Demazeau, I. Presniakov, 57-Fe Mössbauer study of unusual magnetic structure of multiferroic 3R-$AgFeO_2$, Journal of Physics: Condensed Matter 29 (27) (2017) 275803, publisher: IOP Publishing. doi:10.1088/1361-648X/aa70ae.

[38] B. J. Ingram, G. B. González, T. O. Mason, D. Y. Shahriari, A. Barnabè, D. Ko, K. R. Poeppelmeier, Transport and Defect Mechanisms in Cuprous Delafossites. 1. Comparison of Hydrothermal and Standard Solid-State Synthesis in CuAlO2, Chem Mater 16 (26) (2004) 5616–5622. doi:10.1021/cm048983c.

[39] N. Terada, S. Mitsuda, H. Ohsumi, K. Tajima, "Spin-Driven" Crystal Lattice Distortion in Frustrated Magnet CuFeO2: Synchrotron X-ray Diffraction Study, Journal of the Physical Society of Japan 75 (2) (2006) 023602, publisher: The Physical Society of Japan. doi:10.1143/JPSJ.75.023602.

T (K)	Component	fraction (%)	Γ (mm/s)	δ (mm/s)	B_{hf} (T)	ΔE_Q (mm/s)
6	Fe_2O_3	10	0.37	0.48	55.1	0.52
	C1	61(2)	0.44(1)	0.51(1)	53.4(1)	0.65(1)
	C2	14(1)	0.3	0.27(1)	50.9(1)	0.11(1)
	C3	15(1)	0.3	0.36(1)	52.0(1)	0.40(1)
12	Fe_2O_3	10	0.37	0.48	55.1	0.52
	C1	64(2)	0.50(1)	0.51(1)	51.8(1)	0.66(1)
	C2	12(1)	0.25	0.25(1)	49.2(2)	0.08(1)
	C3	14(1)	0.25	0.35(1)	50.6(2)	0.39(2)
14	Fe_2O_3	10	0.37	0.48	55.1	0.52
	C1	71(2)	0.51(2)	0.54(2)	50.8(4)	0.65(1)
	C2	8(1)	0.23	0.26(1)	48.1(4)	0.08(1)
	C3	11(1)	0.23	0.38(1)	49.7(1)	0.37(1)
16	Fe_2O_3	10	0.22	0.48	55.1	0.52
	C1	71(2)	0.56(1)	0.55(1)	49.5(2)	0.67(1)
	C2	6(1)	0.23	0.28(1)	47.5(2)	0.08(1)
	C3	13(1)	0.23	0.42(2)	49.1(1)	0.46(1)
18	Fe_2O_3	10	0.22	0.48	55.1	0.52
	C1	32(2)	0.45(1)	0.49(2)	48.1(1)	0.70(1)
	C2	29(2)	0.70(1)	0.41(1)	44.2(2)	0.10(1)
	C3	29(2)	0.39(1)	0.40(1)	47.9(1)	0.47(1)
20	Fe_2O_3	10	0.22	0.48	55.1	0.52
	C1	26(2)	0.40(4)	0.45(1)	46.6(1)	0.58(3)
	C2	47(3)	0.76(4)	0.43(1)	41.5(1)	0.02(2)
	C3	17(2)	0.44(7)	0.45(1)	44.5(2)	0.45(4)
22	Fe_2O_3	10	0.22	0.48	55.1	0.52
	C1	18(1)	0.50(1)	0.45(1)	43.7(1)	0.54(1)
	C2	26(1)	0.90(1)	0.47(1)	36.9(1)	0.04(2)
	C3	20(1)	0.56(1)	0.45(1)	40.8(1)	0.24(1)
	C4	26(1)	2.8(1)	0.87(3)	10.4(4)	2.5(2)
24	Fe_2O_3	10	0.22	0.48	55.1	0.52
	C1	17(2)	1.0(1)	0.52(3)	38.2(2)	0.2(1)
	C2	48(3)	3.7(5)	0.58(5)	10(2)	0.56(6)
	C3	9(3)	0.8(1)	0.65(3)	29.3(2)	2.3(5)
	C4	16(1)	0.43(1)	0.45(1)	0	0.64(1)
26	Fe_2O_3	10(1)	0.22(2)	0.48(1)	55.1(2)	0.52(2)
	C1	49(1)	4.9(3)	0.3(1)	5(3)	1(1)
	C2	41(1)	0.35(1)	0.45(2)	0	0.62(1)
240	Fe_2O_3	14(1)	0.31(1)	0.42(1)	54.5(1)	0.48(2)
	C1	86(1)	0.41(1)	0.38(1)	0	0.62(1)
270	Fe_2O_3	14(1)	0.37(1)	0.38(1)	54.4(1)	0.43(1)
	C1	86(1)	0.40(1)	0.37(1)	0	0.62(1)

Table 2: Hyperfine parameters obtained by between 6 and 270 K, where Γ is the full width at half maximum of the Lorentzian lineshape, δ is the isomer shift, B_{hf} is the hyperfine magnetic field and ΔE_Q is the quadrupole splitting. Parameters without error indicate that this parameter was fixed in the fitting process.